# Journal of Materials Chemistry A

Accepted Manuscript



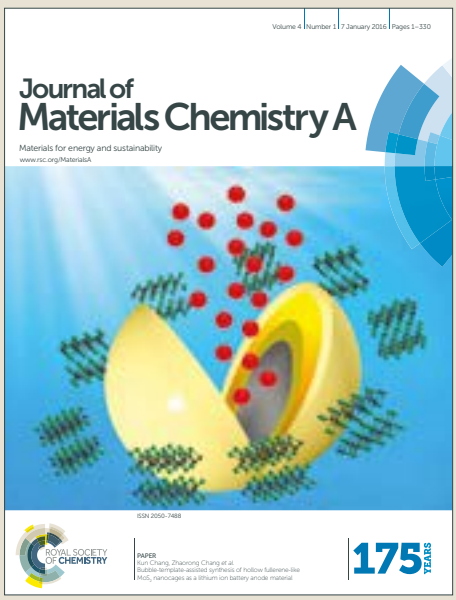




ROYAL SOCIETY OF CHEMISTRY

rsc.li/materials-a

View Article Online
DOI: 10.1039/C9TA01693G

# Direct synthesis of hollow single-crystalline zeolite Beta using a small organic lactam as a recyclable hollow-directing agent

Dongpu Zhao[a,b], Yanan Wang[a,b], Weifeng Chu[a,b], Xinyi Wang[a,c], Xiangxue Zhu[a], Xiujie Li[a], Sujuan Xie[a], Hongxia Wang[c], Shenglin Liu[a]*, and Longya Xu[a]*

[a] *State Key Laboratory of Catalysis, Dalian Institute of Chemical Physics, Chinese Academy of Sciences, Dalian 116023, Liaoning, China*

[b] *University of Chinese Academy of Sciences, Beijing 100049, China*

[c] *Key Laboratory of Photochemical Biomaterials and Energy Storage Materials, College of Chemistry and Chemical Engineering, Harbin Normal University, Harbin, Heilongjiang Province 150025, China*

* Correspondence to: *lyxu@dicp.ac.cn*, *slliu@dicp.ac.cn*



Hollow zeolites are widely investigated as catalysts and nanoreactors in the petrochemical and fine chemical industry because they offer fast mass transfer along with a hollow core for encapsulation of functional components. However, the synthesis of hollow zeolites still remains a significant challenge due to the complexity and restrictions of now available synthetic strategies. Herein, a direct and efficient approach for constructing hollow zeolite Beta with simultaneously low Si/Al ratio (～19) and high yield (above 89 wt%) based on some cost-effective and recyclable pentacyclic lactams, is reported. Meanwhile, a unique formation mechanism involving the selective decomposition of the tetraethylammonium ($TEA^+$) cations locating at internal Al sites, dissolution and recrystallization of the internal activated aluminosilicate species from core to outer surface is proposed for the first time. In addition, the hollow Beta catalyst exhibits better catalytic performance in the alkylation of benzene with isobutylene compared with the conventional solid Beta sample.



## Introduction

View Article Online
DOI: 10.1039/C9TA01693G

Hollow or core-shell micro-/nanomaterials have recently received considerable attention due to their extensive applications in catalysis, biomedicine and electronics.[1-5] The constituents of these micro-/nanostructures can be a broad range of materials such as silica, metal oxides, polymers, zeolites and metal organic frameworks (MOFs).[6] In particular, hollow zeolites possessing excellent diffusivity and unique shape selectivity are widely investigated as catalysts and nanoreactors in the petrochemical and fine chemical industry.[7, 8]

Nonetheless, despite great efforts that have been made over the past decades, practical applications of hollow zeolites are still scarce,[9] as the difficulties in developing facile methods for the direct synthesis of hollow zeolites. So far, a variety of pioneering strategies have been developed to fabricate hollow zeolites, such as the templating method,[10-13] controlled dissolution in the alkaline/acidic solutions[14-17] and dissolution-recrystallization in the presence of structure-directing agents[18-20]. However, these earlier contributions reported concern almost entirely MFI-type zeolites (silicalite-1 and ZSM-5) and involve multiple steps. Thus, a direct and facile synthetic route affording hollow zeolites is highly desired for practical industrial catalytic applications.

We present here a direct synthetic strategy capable of selectively decomposing the tetraethylammonium ($TEA^+$) cations locating at internal Al sites, dissolving and recrystallizing the internal activated aluminosilicate species from core to outer surface, based on some cost-effective and recyclable pentacyclic lactams (P). To the best of our knowledge, this is the first demonstration of some small organic molecules acting as such hollow-directing agents. It is found that the filling of a large number of lactam molecules in zeolite pores and the H-bonding between acylamino groups of lactam and external surface silanols of zeolite restrict the diffusion of external $TEA^+$ (in the mother liquid) into internal decomposed $TEA^+$ sites (locating at internal Al sites) during crystal growth period. Consequently, the internal aluminosilicate species (locating at zeolite core) are activated and tend to be dissolved, migrate out and recrystallize on the outer surface of crystals as the crystallization going on.

View Article Online
DOI: 10.1039/C9TA01693G

Zeolite Beta is a large pore zeolite with two types of intersecting 12-ring channels (0.66 nm × 0.67 nm in [100] and [010], and 0.56 nm × 0.56 nm in [001]).[21, 22] The micropore size of zeolite Beta is larger than that of zeolites ZSM-5 and ZSM-11, which makes it very useful in the petrochemical industry.[23-25] Herein, the catalytic performance of the obtained material is evaluated in the alkylation of benzene with isobutylene. The hollow zeolite Beta catalyst shows improved tert-butylbenzene selectivity by facilitating the diffusion of molecules. This discovery may provide a direct, sustainable and efficient strategy for the synthesis of hollow zeolites that are largely demanded in the chemical industry.



## Experimental section

### Synthesis

**Chemicals and reagents.** Fumed silica (95% $SiO_2$, Shenyang Chemical Co. Ltd, China), sodium aluminate (49% $Al_2O_3$, 38% $Na_2O$, Zibo Tongjie Chemical Co. Ltd, China) and sodium hydroxide (96% NaOH, Sinopharm Chemical Reagent Co. Ltd, China) were used as the sources of Si, Al and inorganic base, respectively. Tetraethylammonium hydroxide (TEAOH, 35% in water, SACHEM) was used as the structure-directing agent. *N*-methyl-2-pyrrolidone (NMP, 99%, Tianjin Kemiou Chemical Reagent Co. Ltd, China), *N*-ethyl-2-pyrrolidone (NEP, 99%, Energy Chemical Reagent Co. Ltd, China) and *N*-isopropyl-2-pyrrolidone (NPP, 99%, Beijing Ouhe Technology Co. Ltd, China) were used as the "hollow-directing agent". All reagents were used as purchased without further purification.

View Article Online
DOI: 10.1039/C9TA01693G

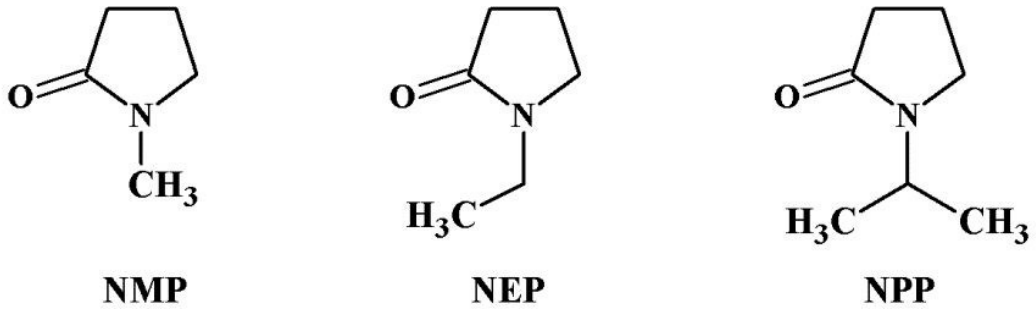


**Scheme 1** Chemical structural formula of NMP, NEP and NPP.



**Synthesis of zeolite Beta.** Hollow Beta crystals were hydrothermally synthesized by a simple one-pot method. A typical gel molar composition is 3.0 NMP/1.0 $SiO_2$/0.023 $Al_2O_3$/0.048 $Na_2O$/0.636 TEAOH/15.6 $H_2O$. In a typical synthesis, 0.4 g of $NaAlO_2$ and 0.13 g of NaOH were first dissolved in the mixed solution of 22.26 g of TEAOH and 5 mL of $H_2O$ with fast stirring. When a clear solution was obtained, 25 g of NMP, 4 mL of $H_2O$ and 5.27 g of fumed silica were added in turn. After stirring for 2 h, the resulting gel was transferred into a 200 mL Teflon-lined stainless steel autoclave. The crystallization was carried out at 140 °C under rotational state (30 rpm). The autoclave was quenched with cold tap water after the prescribed crystallization time. The supernatant was carefully separated from the mother liquor by centrifugation (10000 rpm for twenty minutes). The solid product was centrifuged, washed with distilled water and dried at 100 °C overnight. For comparison, conventional zeolite Beta (denoted as C-Beta) was also synthesized in the absence of lactam by a similar procedure.

The H-form Beta sample was obtained by removing organic species (calcined at 550 °C for 6 h), three consecutive ion exchanges with 1.0 M $NH_4NO_3$ solution at 80 °C (2 h per time) and calcining in air at 550 °C for 6 h.

**Characterization**

X-ray diffraction (XRD) patterns were collected with an Empyrean-100 X-ray diffractometer (PANalytical B. V.) using Cu Kα radiation (λ = 1.5406 Å). Si and Al contents were determined by a PANAlytical Zetium X-ray

View Article Online
DOI: 10.1039/C9TA01693G



fluorescence (XRF) spectrometer. $N_2$ sorption measurements were taken on a Micromeritics ASAP 2020 HD88 surface area and porosity analyzer at -196 °C, previously degassing of the samples were operated at 350 °C for 5 h. Thermal gravimetric analysis (TGA) was carried out on a Pyris Diamond TG/DTA analyser under air flow rate of 40 mL $min^{-1}$ with a ramp rate of 10 °C $min^{-1}$. The FT-IR spectra in the range of 400-1600 $cm^{-1}$ were obtained on a VERTEX 70 FT-IR spectrometer (Bruker Company). Scanning electron microscopy (SEM) was performed on a HITACHI SU1510 microscope operated at 15 kV using samples coated with Pt. Field emission scanning electron microscope (FESEM) was performed on a JSM-7800F electron microscope (JEOL Company) with an acceleration voltage of 0.5 or 1 kV. Transmission electron microscopy (TEM) and selected area electron diffraction (SAED) measurements were observed on a JEM-2100 transmission electron microscope (JEOL Company) equipped with a field emission gun and operating at 200 kV. $^{27}Al$ MAS NMR spectra at a spinning rate of 6 kHz were recorded on an Agilent DD2-500 MHz spectrometer at a $^{27}Al$ frequency of 130.32 MHz with a $\pi/12$ pulse length of 3.2 μs and a recycle delay of 2 s. $^{29}Si$ MAS NMR spectra at a spinning rate of 5 kHz were measured on the same spectrometer at a $^{29}Si$ frequency of 99.37 MHz with a $\pi/2$ pulse length of 5.0 μs and a recycle delay of 4 s. $^{13}C$ MAS NMR spectra were measured using a 4-mm NMR probe at a spinning rate of 5 kHz, corresponding to a frequency of 125.7 MHz. $^{13}C$ liquid-state NMR spectra of the supernatants were recorded at a $^{13}C$ frequency of 125.7 MHz. The acidity of the H form sample was analyzed by temperature-programmed desorption of ammonia ($NH_3$-TPD).

**Catalytic test**

The catalytic performances of the Beta-based catalysts for the alkylation of benzene with isobutylene were tested in a fixed bed reactor. The catalyst (0.5 g, 20-40 mesh) was loaded in the center of a stainless steel reactor and activated in situ at 400 °C for 2 h under $N_2$ flow before starting each reaction run. When the reactor temperature was adjusted down to the reaction temperature of 240 °C, liquid benzene was first pumped in to fill the reactor,

View Article Online
DOI: 10.1039/C9TA01693G

followed by the feeding of isobutylene. The reaction was performed under the conditions of 3.5 MPa, weight hourly space velocity (WHSV) isobutylene of 4 $h^{-1}$, and benzene/isobutylene molar ratio of 4.0. The liquid phase and gas phase products were collected respectively, and analyzed on an Agilent 7890 B GC chromatograph, equipped with a flame ionization detector (FID).

## Results and discussion

**Synthesis and characterization of Ho-Beta.** The XRD patterns (Fig. 1A) of Ho-Beta and C-Beta show peaks characteristic of *BEA-type zeolite, proving the formation of highly crystalline zeolite Beta crystals.[26] The $N_2$ sorption isotherm (Fig. 1B) of Ho-Beta shows a typical H2-type hysteresis loop with an abrupt step around $P/P_0$ = 0.45 in the desorption branch, which is ascribed to capillary condensation of nitrogen within the large voids of Ho-Beta crystals.[19] The textural properties of Ho-Beta and C-Beta are summarized in Table 2. The BET surface area decreases, the micropore volume remains almost the same, while the mesopore volume increases from 0.283 to 0.330 $cm^3\ g^{-1}$ with the appearance of void core.

As revealed by FESEM and TEM images (Fig. 2), Ho-Beta sample with a regular void in the interior, presents an uniform square morphology (with dimensions of 300 nm × 350 nm) and a shell thickness of about 100 nm. Amazingly, despite being composed of abundant nanocrystals (less than 20 nm), each isolated particle is a single crystal. As shown in Fig. 2g-i, the inserted SAED pattern of one individual particle displays a single set of clear diffraction spots, and the corresponding high-resolution transmission electron microscopy (HRTEM) images show clear lattice fringes with consistent orientations over the entire image region, both confirming the single crystal property of Ho-Beta.[27-29] It should be noted that the hollow structure develops until when the $NMP/SiO_2$ molar ratio is higher than 3.0 in the starting gel (Fig. S1).

View Article Online
DOI: 10.1039/C9TA01693G



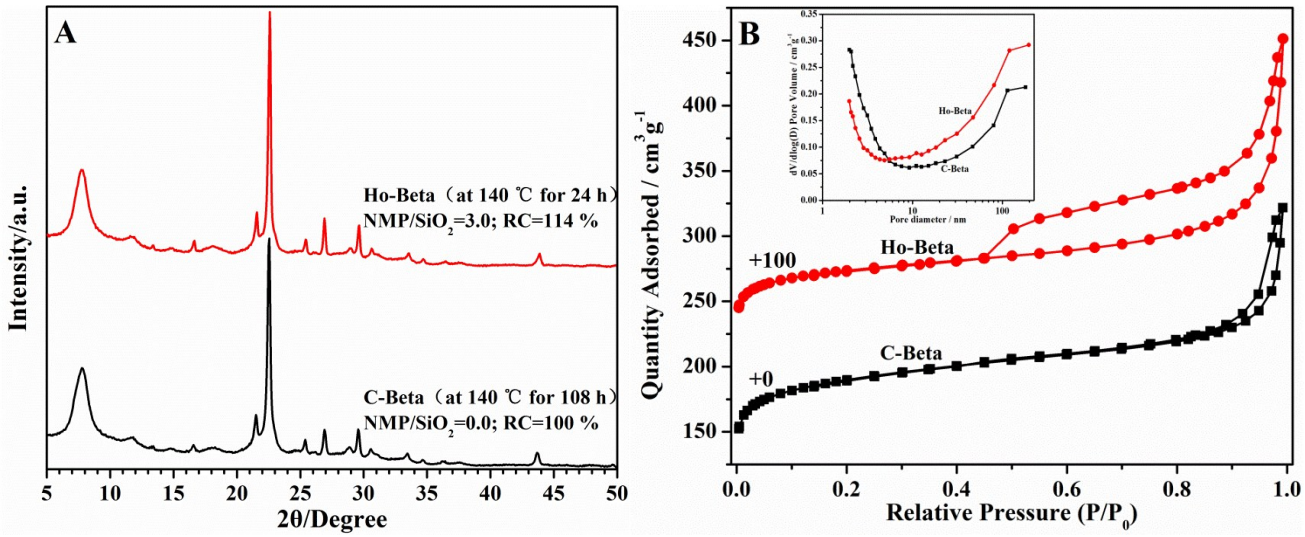


**Fig. 1** (A) XRD patterns and (B) nitrogen sorption isotherms of Ho-Beta and C-Beta.

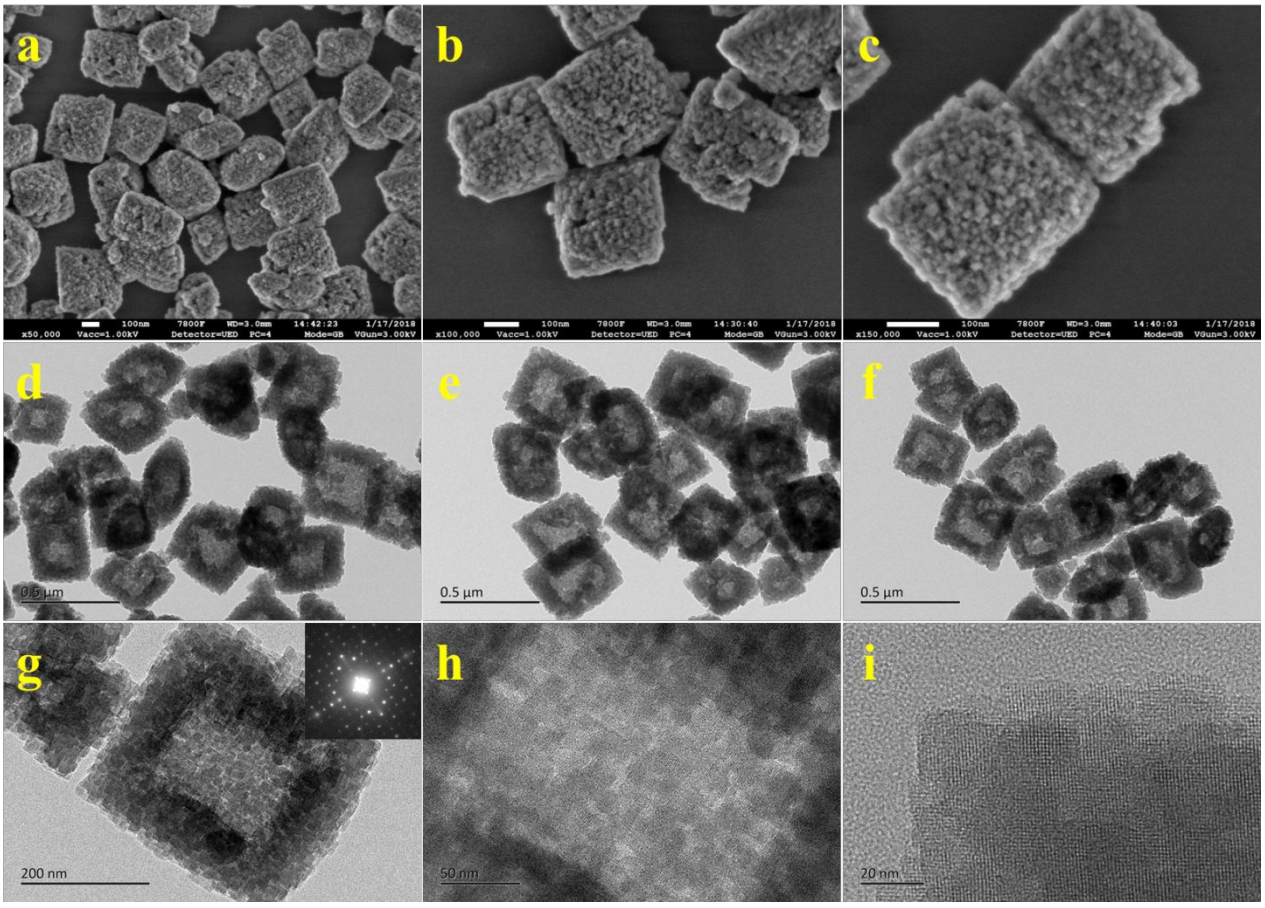


**Fig. 2** (a-c) FESEM images of as-synthesized Ho-Beta at different magnifications. (d-f) TEM images of as-synthesized Ho-Beta obtained in different areas. (g) TEM image and SAED pattern of one individual Ho-Beta

View Article Online
DOI: 10.1039/C9TA01693G

crystal. (h) HRTEM image of the central zone of the as-synthesized Ho-Beta crystal. (i) HRTEM image of the rim of the as-synthesized Ho-Beta crystal.

Meanwhile, we find that the other two analogues of NMP, NEP and NPP (Scheme 1), are also capable of inducing the formation of hollow single-crystalline zeolite Beta, as shown in Fig. 3 and S2. Clearly, the above results suggest that these pentacyclic lactams play a critical role in the formation process of hollow zeolite Beta.



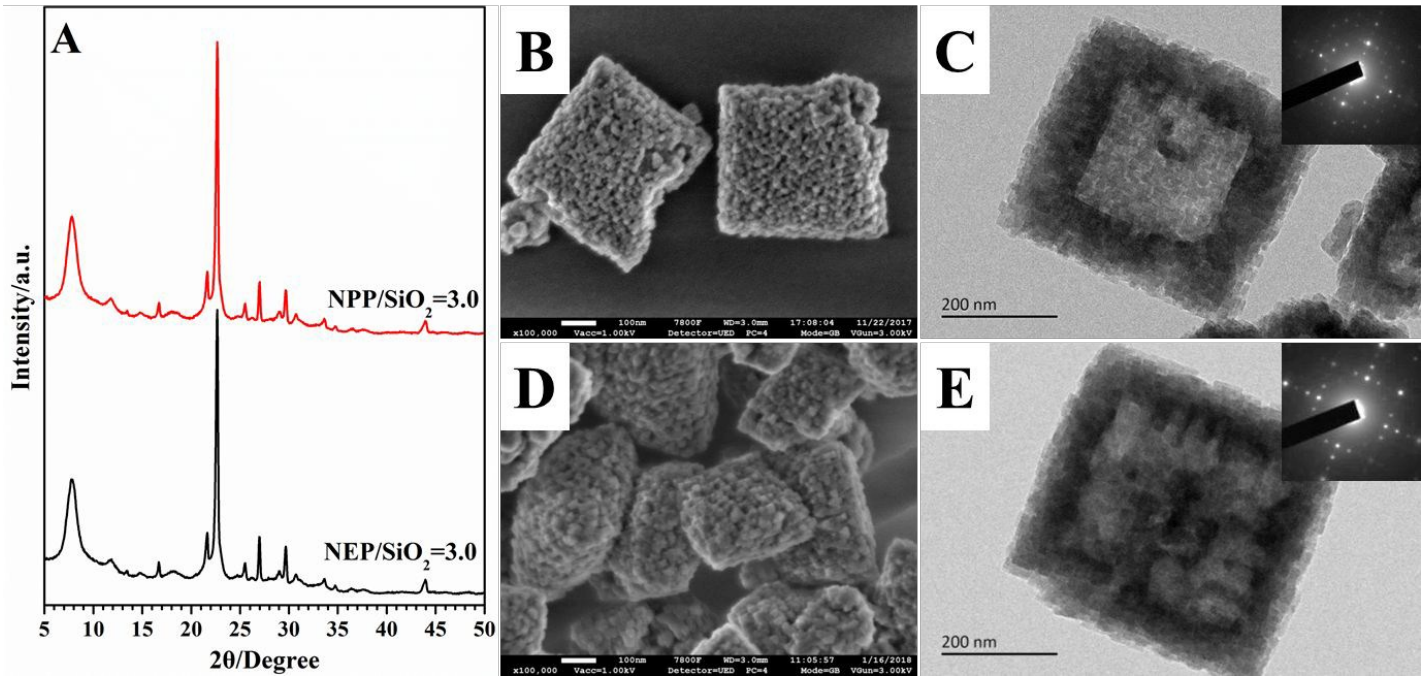


**Fig. 3** (A) XRD patterns, FESEM and TEM images of the hollow zeolites Beta synthesized with NEP/$SiO_2$ = 3.0 (B and C) and NPP/$SiO_2$ = 3.0 (D and E), respectively. Gel molar composition: 3.0 P/1.0 $SiO_2$/0.023 $Al_2O_3$/0.048 $Na_2O$/0.636 TEAOH/15.6 $H_2O$ (P: NEP or NPP).

**Insight into the formation mechanism of Ho-Beta.** The formation process of Ho-Beta is tracked by XRD, FESEM and TEM. The XRD patterns (Fig. S3A) show that no crystalline phase is detected in the first 3 h. Characteristic diffraction peaks attributed to zeolite Beta are first observed after 12 h of heating. The diffraction

View Article Online
DOI: 10.1039/C9TA01693G

peaks are intensified gradually between 12 h and 21 h. Further prolonging hydrothermal time from 24 h to 60 h, the products are still highly crystalline zeolite Beta and the crystallinity keeps constant (Fig. S3B). In contrast, when the synthesis is performed without NMP, fully crystalline Beta develops until 108 h (as shown in Fig. S4).

The FESEM images (Fig. S5) show that the initial product (0 h) consists of amorphous nanoparticles with diameter 10-15 nm. These tiny particles evolve to larger particles with diameter about 32 nm after 3 h of heating. After the onset of crystallization (12 h), bits of square crystals emerge. More and larger crystals form as the crystallization time increases to 18 h. At the end of the synthesis (21-24 h), the amorphous nanoparticles are completely consumed and grow into uniform square-like crystals.

According to TEM (Fig. S6), square-like crystals together with amorphous matrixes are observed in the sample crystallized for 18 h. However, no cavity generate in the interior of these crystals. A fascinating change in the interior happens between 21 h and 24 h, when the exterior particle size only increases slightly. At 21 h, all the amorphous matrixes disappear, and only submicron-sized crystals can be found. At the same time, indistinct core-shell structure evolves as exemplified in Fig. S6E. At 24 h, obvious square void and dense shell develop. Further hydrothermal treatment to 60 h, the hollow structure is well maintained. These results suggest that the hollow core forms by consuming the crystalline nutriments locating in the zeolite core.

$^{13}$C NMR measurements (Fig. 4 and S7) are carried out to unveil the function of NMP in the formation process of Ho-Beta. In the presence of NMP, the $^{13}$C NMR spectrum of the supernatant before hydrothermal synthesis (0 h) exhibits some peaks attributed to *N*-methyl-4-aminobutyrate anions (the ring-opening product of NMP, marked as ①, ②, ③, ④ and ⑤), in addition to aqueous TEAOH (marked as a and b) and NMP (marked as 1, 2, 3, 4 and 5). After 12 h of hydrothermal treatment, two peaks associated with trimethylamine (TEA, the Hoffmann degradation product of TEAOH; marked as I and II) appear. Upon heating 18 h, the intensities of the peaks assigned to TEA and *N*-methyl-4-aminobutyrate anions increase slightly. Further heating from 21 h to 60

View Article Online
DOI: 10.1039/C9TA01693G

h, the peak intensities of TEA increase, while those of *N*-methyl-4-aminobutyrate anions decrease, implying the self-repairing function of NMP and the thermal instability of TEAOH. Based on the above results, we conjecture that partial NMP molecules initial dissociate to *N*-methyl-4-aminobutyrate anions in the highly alkaline synthetic gel. Nevertheless, the Hoffmann degradation of TEAOH at high temperature, yields TEA while lowers the $OH^-$ concentration in the synthesis mixture; consequently, *N*-methyl-4-aminobutyrate anions self-heal back to NMP again (Fig. 4D). The solid-state $^{13}C$ NMR spectrum (Fig. 4B) of the final product show that only peaks associated with $TEA^+$ species appear, suggesting that the NMP molecules are only physically filled in the zeolite pores and/or weakly interacted with the zeolite surface.

Likewise, in the conventional synthetic system, the degradation amount of TEAOH also increases with the extending of hydrothermal time (Fig. S7A), and only $TEA^+$ exist in the final product (see Fig. S7B). However, seen from Fig. S8, the degradation of TEAOH is obviously accelerated (about five times faster) by the introduction of NMP. The above results demonstrate that the presence of NMP accelerates both the crystallization of zeolite Beta and the degradation of TEAOH.

View Article Online
DOI: 10.1039/C9TA01693G



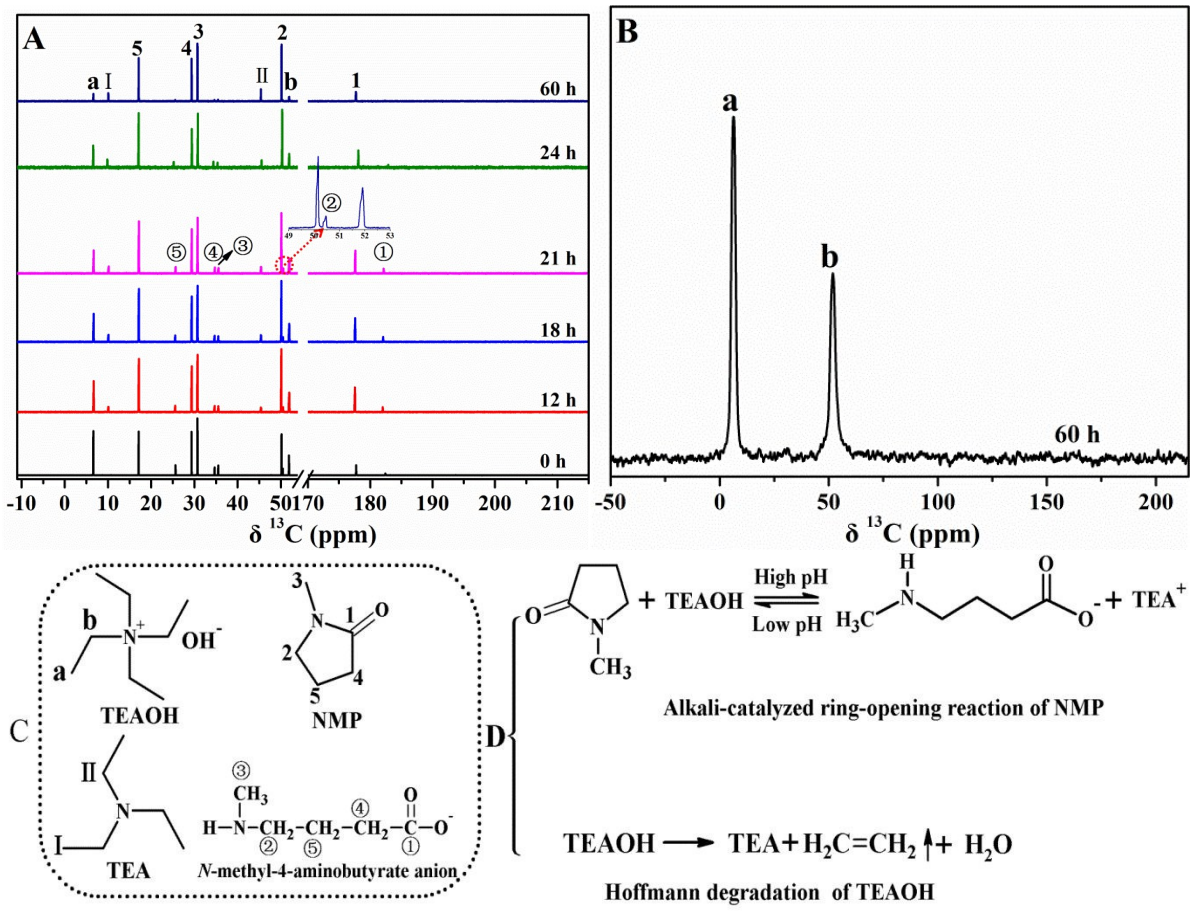


**Fig. 4** (A) Liquid-state $^{13}C$ NMR spectra of the supernatants. (B) Solid-state $^{13}C$ NMR spectrum of the final product. (C) Chemical structures of TEAOH, NMP, TEA and *N*-methyl-4-aminobutyrate anion. (D) The alkali-catalyzed ring-opening reaction of NMP, and the Hoffmann degradation of TEAOH.

Fig. 5 and S9, and Table 1 summarize the thermogravimetric (TG) and differential thermogravimetric (DTG) analyses results of the samples synthesized with and without NMP. In the presence of NMP, the weight loss assigned to $TEA^+$ increases with the prolonging of synthesis time before 12 h. After the onset of crystallization (12 h), the weight loss corresponding to $TEA^+$ remains almost constant. In comparison with the conventional counterparts synthesized without NMP, it can be found that the presence NMP enhances the combination rate of the activated $TEA^+$ with aluminosilicates. This is mainly due to the fact that, as discussed previously,[30] TEAOH

View Article Online
DOI: 10.1039/C9TA01693G

can be dissociated by NMP (Fig. 4D), leading to the fast release of the activated $TEA^+$ and its subsequent incorporation with negatively charged aluminosilicates.

DTG characterization (Fig. 5B and S9B) enables us to identify the distribution sites of the occluded $TEA^+$ species. According to the references,[31, 32] the DTG curves can be divided into three stages: (1) weight loss blow 150 °C is assigned to the desorption of water; (2) weight loss at 150-400 °C is due to the decomposition of $TEA^+$ balancing at surface silanol defects ( $\equiv Si - O^- \cdots HOSi \equiv$ ); (3) weight loss above 400 °C is attributed to the decomposition of $TEA^+$ balancing negatively charged Al sites ( $\equiv Si - O^- - Al \equiv$ ). Obviously, the presence of NMP in the synthetic gel strongly influences the distribution of $TEA^+$.

In the presence of NMP, the occluded $TEA^+$ species before heating absolutely locate at surface silanol defects. Upon the crystallization time increases from 3 h to 18 h, a small quantity of $TEA^+$ species locating at negatively charged Al sites emerge. Meanwhile, the weight loss of the $TEA^+$ species locating at Al sites decreases from 4.76 wt% to 2.02 wt%, and finally to 0.96 wt%; while the weight loss of those locating at surface silanol defects increases from 11.66 wt% to 18.18 wt%, and finally to 18.24 wt% at the same time. This result clearly indicates that the $TEA^+$ species locating at Al sites decompose gradually during this stage. At the end of crystallization (18-24 h), the weight loss of the $TEA^+$ species locating at surface silanol defects decreases, along with an increase for those locating at Al sites, indicating the rearrangement of $TEA^+$. Moreover, it can also be found that the decomposition temperature of the $TEA^+$ species locating at Al sites shifts from 440 °C to 420 °C when the crystallization time ranges from 18 h to 21 h, in contrary to that observed in a conventional synthetic system.[32] Combined with the TEM observation, the phenomenon presented above can be ascribed to the migration of internal aluminosilicate species from core to outer surface, because the $TEA^+$ species locating at zeolite surface are easier to decompose than those locating at zeolite core. While, in the absence of NMP, the occluded $TEA^+$

View Article Online
DOI: 10.1039/C9TA01693G

mostly locates at Al sites and its weight loss increases with the prolonging of crystallization time, as shown in Fig. S9 and Table 1.

The effect of NMP on the distribution and rearrangement of $TEA^+$ can be ascribed to the filling of a large number of NMP molecules in zeolite pores and the H-bonding between acylamino groups of NMP and external surface silanols of zeolite,[28] which restrict the diffusion and compensation of external $TEA^+$ (in the mother liquid) into internal decomposed $TEA^+$ sites (locating at internal Al sites). As is well known, the $TEA^+$ cations entrapped in zeolite not only compensate the negatively charged Al sites, but also stabilize the zeolite framework. Therefore, the decomposition of internal $TEA^+$ will activate the aluminosilicate species locating at zeolite core, thus dissolution and recrystallization of internal aluminosilicate species from core to surface may occur in the highly alkaline media.[33] In contrast, when the synthesis is performed under NMP/$SiO_2$ molar ratios lower than 3.0, the equilibrium between the internal decomposed $TEA^+$ and the external introduced $TEA^+$ can still be achieved; therefore the aluminosilicate species locating at zeolite core are stable enough.

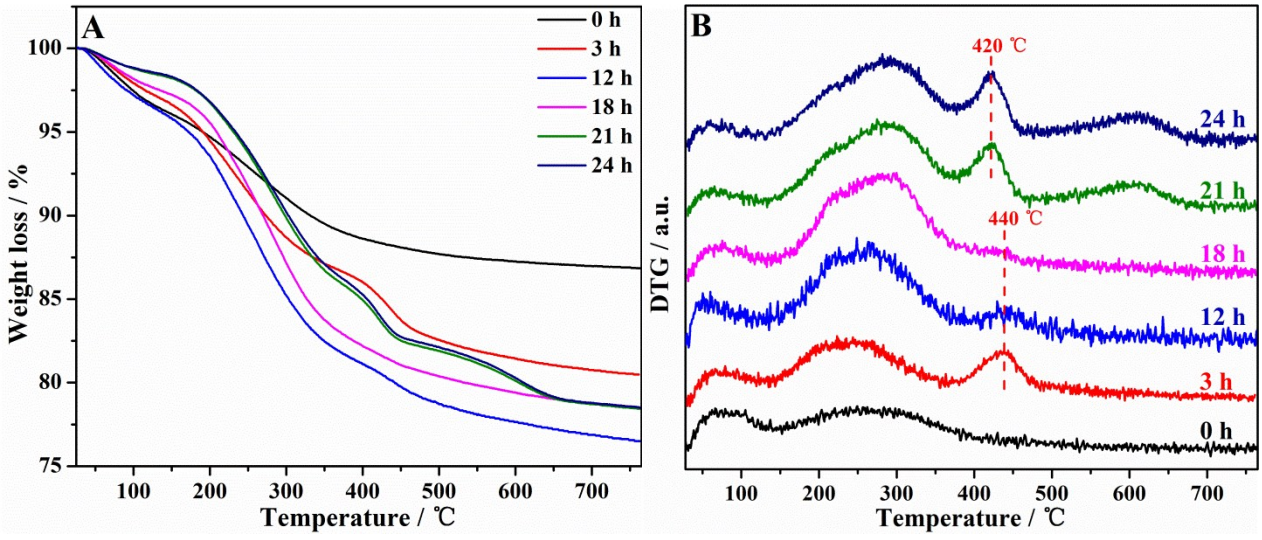


**Fig. 5** (A) TG and (B) DTG curves of the products synthesized with NMP for different periods of time.

View Article Online
DOI: 10.1039/C9TA01693G

To verify the existence of abundant surface silanol defects in Ho-Beta, FT-IR technique is also applied to study the framework vibrations of the calcined Ho-Beta and C-Beta samples. As shown in Fig. 6, both samples exhibit almost identical absorption bands belonging to well crystalline zeolite Beta. While, a new band centered at 958 $cm^{-1}$ appears for Ho-Beta compared to C-Beta, which is usually recognized as a sign of rich surface silanol defects in zeolite,[34] in good agreement with the DTG analysis result.

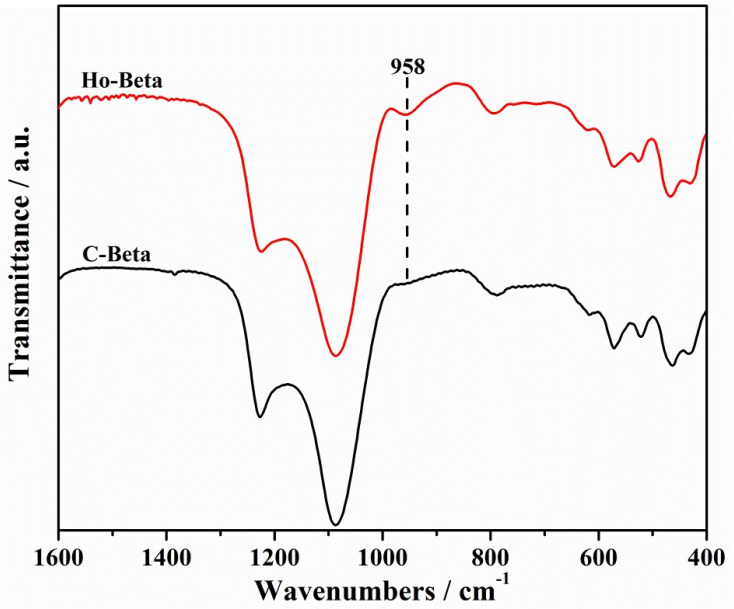


**Fig. 6** FT-IR spectra of the calcined C-Beta and Ho-Beta samples.

$^{27}Al$ and $^{29}Si$ MAS NMR measurements are conducted to trace the chemical states of silicon and aluminum species. As depicted in Fig. 7A, only one peak centered at around 54 ppm, stemming from four-coordinated aluminum species, is detected throughout the synthesis. It should be noted that the full width at half-maximum (fwhm) of the four-coordinated aluminum species decreases gradually during the crystal growth period (12-21 h), implying the formation of more ordered aluminosilicates structure.[32]

View Article Online
DOI: 10.1039/C9TA01693G

$^{29}$Si MAS NMR spectra are given in Fig. 7B. All samples show four resonances at around -115, -110, -105 and -100 ppm. The resonances at -115 and -110 ppm are correspondent to $Q^4$(0Al) ($Si(OSi)_4$); the resonance at -105 ppm is assigned to both $Q^3$(1Al) ($Si(OSi)_3(OAl)_1$) and $Q^3$(0Al) ($Si(OSi)_3(OH)_1$); the resonance at -100 ppm is attributed to $Q^2$(2Al) ($Si(OSi)_2(OAl)_2$), $Q^2$(1Al) ($Si(OSi)_2(OAl)_1(OH)_1$), and/or $Q^2$(0Al) ($Si(OSi)_2(OH)_2$).[35, 36] Rapid increase in the $Q^4/(Q^2 + Q^3 + Q^4)$ area ratio is observed upon hydrothermal treatment from 12 h to 21 h, suggesting the condensation of silicate species. While further hydrothermal treatment up to 24 h results in a slight decrease in the $Q^4/(Q^2 + Q^3 + Q^4)$ area ratio, indicating the depolymerization of partial silicates.

**Fig. 7** (A) $^{27}$Al and (B) $^{29}$Si NMR spectra of the Ho-Beta samples obtained at different crystallization times.

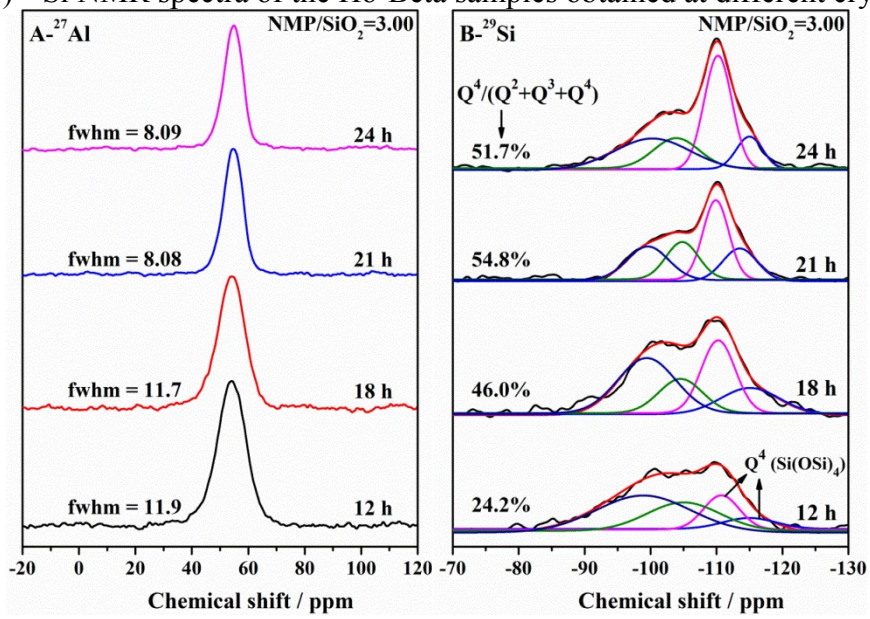


Chemical compositions of the as-synthesized samples are listed in Table 1. The relatively low solid yield in the early stage of synthesis (0-3 h) should be ascribed to the depolymerization of silica[37] and the subsequent co-condensation of silicate and aluminate, as it can be deduced from the changes in Si and Al yields. Meanwhile, increasing amount of $TEA^+$ species are occluded in the products at this stage, suggesting the formation of $TEA^+$-aluminosilicate composites.

View Article Online
DOI: 10.1039/C9TA01693G

With increased synthesis time (12-21 h), the solid yield increases linearly. In combination with the NMR and XRD analyses, the marked change in chemical composition during this period can be due to the condensation of silicate species. Further hydrothermal treatment up to 24 h causes a slight decrease in the Si/Al ratio of the product, additionally confirming the depolymerization of partial silicates, in line with $^{29}$Si MAS NMR analysis. It is noteworthy that despite the hollow structure is indistinct for the sample synthesized at 21 h, its solid yield (89.2 wt%) is extremely close to that obtained at 24 h (89.1 wt%), implying that the hollow structure forms by consuming the aluminosilicate species in the crystals core. Additionally, it can also be found that the final product yield (89 wt% versus 49 wt%) and Si/Al ratio (18.5 versus 12.0) of Ho-Beta are noticeably higher than those of C-Beta. A plausible explanation is that the addition of NMP lowers the pH of the synthetic gel by interacting with TEAOH (see Fig. 4D) and accelerating the decomposition of TEAOH (see Fig. S8). Consequently, the ability of silicon atoms to incorporate into the zeolite framework is enhanced.[30]





**Table 1** Solid yields and chemical compositions of the products synthesized for different periods of time[a]

| sample | synthesis | Si/Al | solid | Si | Al | $TEA^+$ weight | $TEA^+$ distribution (wt%) |
|---|---|---|---|---|---|---|---|

View Article Online
DOI: 10.1039/C9TA01693G

| | time (h) | ratio | yield[b] (wt%) | yield (wt%) | yield (wt%) | loss (wt%) | silanol defects | Al sites |
|---|---|---|---|---|---|---|---|---|
| $NMP/SiO_2$ = 3.0 | 0 | 17.0 | 57.9 | 56.8 | 72.4 | 9.64 | 9.64 | 0.00 |
| | 3 | 10.4 | 49.6 | 47.0 | 98.4 | 16.43 | 11.66 | 4.76 |
| | 12 | 15.7 | 69.6 | 68.0 | 94.1 | 20.20 | 18.18 | 2.02 |
| | 18 | 16.9 | 80.3 | 78.8 | 99.9 | 19.20 | 18.24 | 0.96 |
| | 21 | 19.0 | 89.2 | 88.1 | 99.9 | 20.27 | 14.59 | 5.68 |
| | 24 | 18.5 | 89.1 | 88.0 | 99.9 | 20.27 | 14.39 | 5.88 |
| $NMP/SiO_2$ = 0.0 | 0 | 17.1 | 25.6 | 25.1 | 31.9 | 5.47 | 5.47 | 0.00 |
| | 3 | 3.9 | 2.4 | 2.0 | 11.2 | 7.24 | 0.00 | 7.24 |
| | 60 | 5.9 | 19.5 | 17.4 | 64.0 | 15.31 | 2.69 | 12.83 |
| | 102 | 7.8 | 33.0 | 30.5 | 84.8 | 15.75 | 4.15 | 11.82 |
| | 108 | 12.0 | 49.3 | 47.3 | 85.4 | 19.12 | 4.34 | 15.19 |

[a]Si and Al contents were quantified by XRF, while $TEA^+$ amounts were determined by TGA. [b]Calculated based on oxides (excluding $TEA^+$, $Na_2O$, $H_2O$ and other impurities).

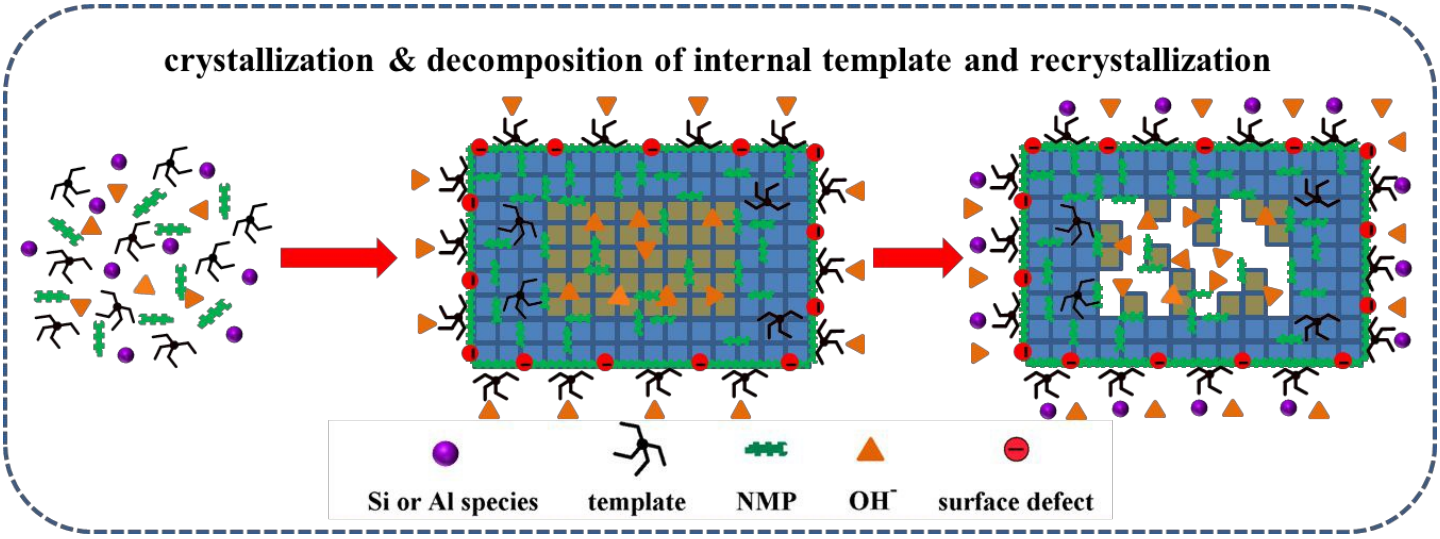


**Fig. 8** Proposed formation process of Ho-Beta via NMP-assisted approach.

Based on the above observations, a novel formation mechanism of hollow Beta crystals is proposed and illustrated in Fig. 8. The $TEA^+$ species locating at internal Al sites decompose along with the crystallization of metastable solid Beta crystals, which leads to the activation of the internal aluminosilicates. As a result, at the subsequent hydrothermal process, the internal activated aluminosilicates tend to be dissolved, migrate out and

View Article Online
DOI: 10.1039/C9TA01693G

recrystallize on the outer surface of Beta crystals in the highly alkaline media, due to the absence of $TEA^+$ protection. In these processes, NMP serves as both promoter to accelerate the dissociation and decomposition of TEAOH and inhibitor to limit the diffusion and compensation of external $TEA^+$ (in the mother liquid) into internal decomposed $TEA^+$ sites (locating at internal Al sites).

In comparison with the hollow zeolite Beta fabricated by templating method[11] and controlled dissolution[33], the approach discovered here is obviously more efficient, convenient and economical.

**Evaluation of catalytic performance.** The catalytic properties of the Beta catalysts are investigated for the alkylation of benzene with isobutylene. Considering that the alkylation reaction is a typical acid catalyzed process,[38, 39] and the lifetime of catalyst and product selectivity are influenced by multiple factors, such as acidity, porosity, crystal size, and reaction conditions. Therefore, a commercial Beta catalyst (denoted as L-Beta, provided by Fushun Petroleum Company; the XRD pattern, SEM image and $N_2$ sorption isotherm are shown in Fig. S11) possessing a similar Si/Al ratio (～19.2), crystal size and acidity with that of Ho-Beta, is also tested with this reaction under the same reaction conditions.

**Table 2** Textural parameters and of Ho-Beta, C-Beta and L-Beta

| sample | $S_{BET}$ ($m^2/g$) | $V_{micro}$ ($cm^3/g$) | $S_{ext}$ ($m^2/g$) | $V_{meso}$ ($cm^3/g$) |
|---|---|---|---|---|
| Ho-Beta | 675 | 0.213 | 127 | 0.330 |
| C-Beta | 728 | 0.215 | 180 | 0.283 |
| L-Beta | 628 | 0.193 | 132 | 0.295 |

View Article Online
DOI: 10.1039/C9TA01693G



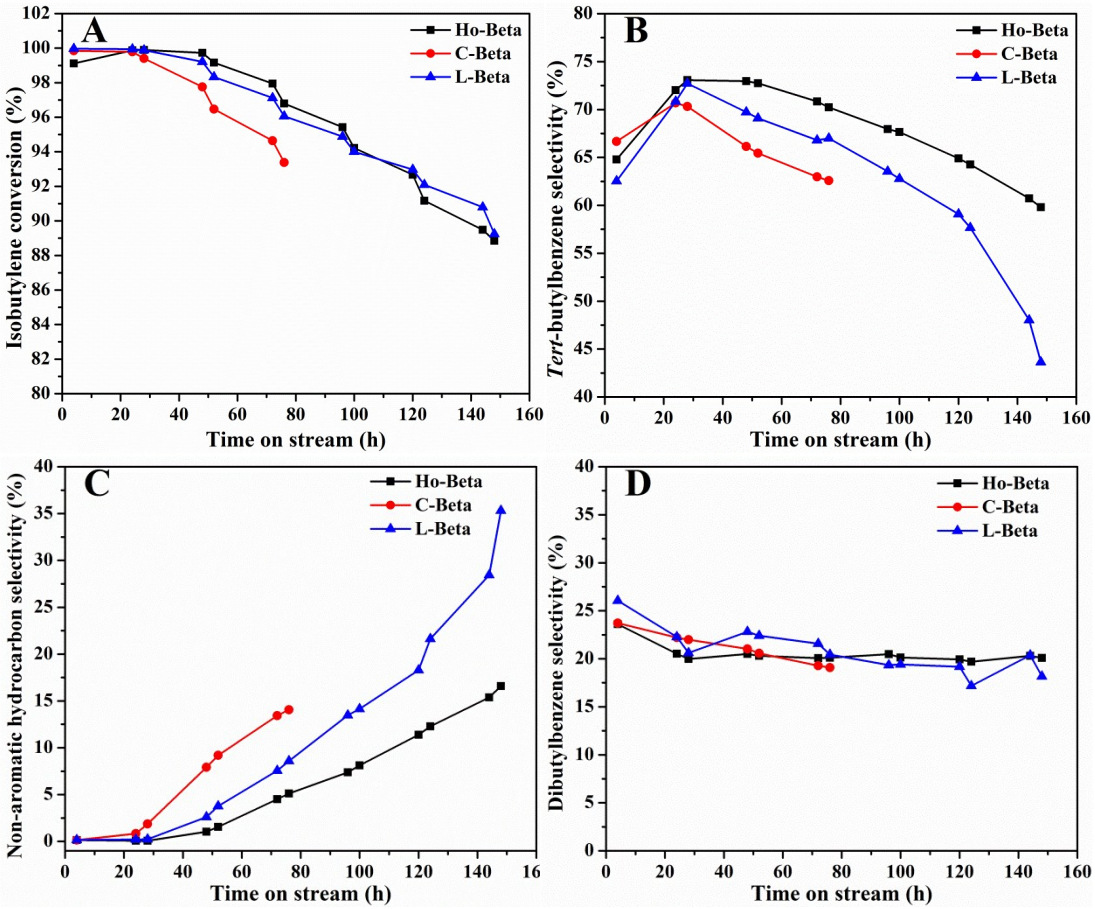


**Fig. 9** Isobutylene conversion and product selectivity as a function of time on stream over Ho-Beta, C-Beta and L-Beta.

**Table 3** Catalytic performances of the Beta catalysts for the alkylation of benzene with isobutylene

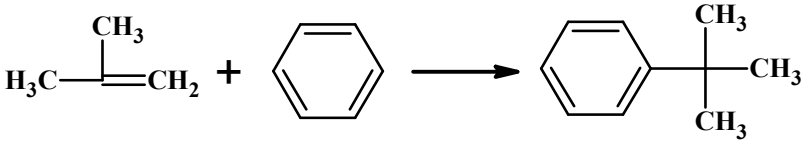

| catalyst | lifetime[a] (h) | selectivity[b] (%) | | | |
|---|---|---|---|---|---|
| | | tert-butylbenzene | dibutylbenzene | non-aromatic hydrocarbons | others[c] |
| Ho-Beta | 100 | 71.0 | 20.7 | 1.8 | 6.5 |
| L-Beta | 100 | 68.3 | 22.3 | 3.3 | 6.1 |
| C-Beta | 72 | 66.4 | 21.1 | 6.8 | 5.7 |

[a]Isobutylene conversion above 94%. [b]Data were collected as the average of the first 76 h. [c]isobutylbenzene and sec-butylbenzene.

View Article Online
DOI: 10.1039/C9TA01693G



The isobutylene conversion and product selectivity are given in Fig. 9 and Table 3. All the three catalysts show above 99% isobutylene conversion at the initial stages, but different catalytic stability with time on stream. The isobutylene conversion and tert-butylbenzene selectivity over C-Beta catalyst drop faster than those over Ho-Beta and L-Beta catalysts, indicating the occurrence of fast catalyst deactivation. Since these three catalysts possess similar crystal size, the poorest catalytic performance of C-Beta catalyst can be attributed to its too much higher acid density (as shown in Fig. S10), resulting in fast coke deposition.

Interestingly, although Ho-Beta and L-Beta catalysts exhibit comparable catalytic activity throughout the catalytic process, the tert-butylbenzene selectivity over Ho-Beta is higher than that over L-Beta. This may benefit from the improved transport properties of Ho-Beta. As is well known, the existence of internal cavity in the zeolite crystal can enormously shorten the diffusion path for the reactants and products,[9, 14, 28] consequently the side reaction (the self-polymerization of isobutylene, which produces non-aromatic hydrocarbons) is inhibited and a higher tert-butylbenzene selectivity is achieved. Clearly, the above results demonstrate that the hollow zeolite Beta is an ideal catalyst for the alkylation of benzene with isobutylene.

## Conclusions

Hollow single-crystalline zeolite Beta with simultaneously high yield and low Si/Al ratio has been directly synthesized by using some small organic lactams as economical and recyclable hollow-directing agents. Meanwhile, a unique formation mechanism involving the selective decomposition of $TEA^+$ cations locating at internal Al sites, dissolution and recrystallization of the internal activated aluminosilicate species from core to outer surface is revealed. In these processes, NMP serves as both promoter to accelerate the dissociation and decomposition of TEAOH and inhibitor to limit the diffusion and compensation of external $TEA^+$ into internal

View Article Online
DOI: 10.1039/C9TA01693G

decomposed $TEA^+$ sites (locating at internal Al sites). The hollow zeolite Beta catalyst exhibits excellent catalytic property in the alkylation of benzene with isobutylene due to improved diffusion. Work is under way to encapsulate functional metal nanoparticles into hollow zeolite Beta for advanced applications and expand this strategy for preparing hollow zeolite single crystals of other topologies.

## Conflicts of interest

There are no conflicts of interest to declare.



## Acknowledgements

This work was supported by the National Natural Science Foundation of China (No.21773233), Natural Science Foundation of Liaoning Province (201602740), DICP ZZBS201806, K.C. Wong Education Foundation, Dalian Eminent Young Scientist Program (2015R009) and CNPC-DICP Joint Research Center. The authors are grateful to SACHEM Americas company for supplying us TEAOH.

## Notes and references

1 X. Wang, J. Feng, Y. Bai, Q. Zhang and Y. Yin, *Chem. Rev.*, 2016, **116**, 10983-11060.

2 J. Hu, M. Chen, X. Fang and L. Wu, *Chem. Soc. Rev.*, 2011, **40**, 5472-5491.

3 B. Li and H.-C. Zeng, *Adv. Mater.*, 2018, 1801104.

4 T. Li, Y. Liu, S. Qi, X. Liu, L. Huang and L. Sun, *J. Colloid Interface Sci.*, 2018, **526**, 366-373.

5 P. Tan, J. Qin, X. Liu, X. Yin and L. Sun, *J. Mater. Chem. A*, 2014, **2**, 4698-4705.

6 W. Zhu, Z. Chen, Y. Pan, R. Dai, Y. Wu, Z. Zhuang, D. Wang, Q. Peng, C. Chen and Y. Li, *Adv. Mater.*, 2018, 1800426.

View Article Online
DOI: 10.1039/C9TA01693G

7 H. J. Cho, D. Kim, J. Li, D. Su and B. Xu, *J. Am. Chem. Soc.*, 2018, **140**, 13514-13520.

8 J. Zhang, S. Bai, Z. Chen, Y. Wang, L. Dong, H. Zheng, F. Cai and M. Hong, *J. Mater. Chem. A*, 2017, **5**, 20757-20764.

9 C. Pagis, A. R. M. Prates, D. Farrusseng, N. Bats and A. Tuel, *Chem. Mater.*, 2016, **28**, 5205-5223.

10 N. Chu, J. Wang, Y. Zhang, J. Yang, J. Lu and D. Yin, *Chem. Mater.*, 2010, **22**, 2757-2763.

11 Z. Zheng, C. Sun, R. Dai, S. Wang, X. Wu, X. An and X. Xie, *Catal. Sci. Technol.*, 2016, **6**, 6472-6475.

12 X. Wang, W. Yang, Y. Tang, Y. Wang, S. Fu and Z. Gao, *Chem. Commun.*, 2000, 2161-2162.

13 N. Yue, M. Xue and S. Qiu, *Inorg. Chem. Commun.*, 2011, **14**, 1233-1236.

14 C. Mei, Z. Liu, P. Wen, Z. Xie, W. Hua and Z. Gao, *J. Mater. Chem.*, 2008, **18**, 3496-3500.

15 J. C. Groen, T. Bach, U. Ziese, A. Donk, K. P. de Jong, J. A. Moulijn and J. Perez-Ramirez, *J. Am. Chem. Soc.*, 2005, **127**, 10792-10793.

16 D. Fodor, T. Ishikawa, F. Krumeich and J. A. van Bokhoven, *Adv. Mater.*, 2015, **27**, 1919-1923.

17 Y. Qiao, M. Yang, B. Gao, L. Wang, P. Tian, S. Xu and Z. Liu, *Chem. Commun.*, 2016, **52**, 5718-5721.

18 C. Dai, A. Zhang, M. Liu, X. Guo and C. Song, *Adv. Funct. Mater.*, 2015, **25**, 7479-7487.

19 C. Dai, A. Zhang, L. Li, K. Hou, F. Ding, J. Li, D. Mu, C. Song, M. Liu and X. Guo, *Chem. Mater.*, 2013, **25**, 4197-4205.

20 C. Dai, S. Zhang, A. Zhang, C. Song, C. Shi and X. Guo, *J. Mater. Chem. A*, 2015, **3**, 16461-16468.

21 M. M. J. Treacy and J. M. Newsam, *Nature*, 1988, **332**, 249-251.

22 P. S. Barcia, J. A. C. Silva and A. E. Rodrigues, *Microporous Mesoporous Mater.*, 2005, **79**, 145-163.

23 H. Wei, K. Liu, S. Xie, W. Xin, X. Li, S. Liu and L. Xu, *J. Catal.*, 2013, **307**, 103-110.

24 X. Li, W. Zhang, S. Liu, L. Xu, X. Han and X. Bao, *J. Phys. Chem. C*, 2008, **112**, 5955-5960.

25 B. Tang, W. Dai, G. Wu, N. Guan, L. Li and M. Hunger, *ACS Catal.*, 2014, **4**, 2801-2810.

View Article Online
DOI: 10.1039/C9TA01693G

26 F.-S. Xiao, L. Wang, C. Yin, K. Lin, Y. Di, J. Li, R. Xu, D. S. Su, R. Schlogl, T. Yokoi and T. Tatsumi, *Angew. Chem. Int. Ed.*, 2006, **45**, 3090-3093.

27 J. Zhu, Y. Zhu, L. Zhu, M. Rigutto, A. van der Made, C. Yang, S. Pan, L. Wang, L. Zhu, Y. Jin, Q. Sun, Q. Wu, X. Meng, D. Zhang, Y. Han, J. Li, Y. Chu, A. Zheng, S. Qiu, X. Zheng and F.-S. Xiao, *J. Am. Chem. Soc.*, 2014, **136**, 2503-2510.

28 Q. Zhang, G. Chen, Y. Wang, M. Chen, G. Guo, J. Shi, J. Luo and J. Yu, *Chem. Mater.*, 2018, **30**, 2750-2758.

29 C. J. H. Jacobsen, C. Madsen, J. Houzvicka, I. Schmidt and A. Carlsson, *J. Am. Chem. Soc.*, 2000, **122**, 7116-7117.

30 D. Zhao, W. Chu, Y. Wang, X. Zhu, X. Li, J. An, W. Xin, S. Liu and L. Xu, *J. Mater. Chem. A*, 2018, **6**, 24614-24624.

31 M. A. Camblor, A. Corma and S. Valencia, *Microporous Mesoporous Mater.*, 1998, **25**, 59-74.

32 T. Ikuno, W. Chaikittisilp, Z. Liu, T. Iida, Y. Yanaba, T. Yoshikawa, S. Kohara, T. Wakihara and T. Okubo, *J. Am. Chem. Soc.*, 2015, **137**, 14533-14544.

33 K. Iyoki, K. Itabashi and T. Okubo, *Chem. Asian J.*, 2013, **8**, 1419-1427.

34 S. Song, L. Di, G. Wu, W. Dai, N. Guan and L. Li, *Appl. Catal., B*, 2017, **205**, 393-403.

35 H. Jon, N. Ikawa, Y. Oumi and T. Sano, *Chem. Mater.*, 2008, **20**, 4135-4141.

36 H. Zhang, B. Xie, X. Meng, U. Mueller, B. Yilmaz, M. Feyen, S. Maurer, H. Gies, T. Tatsumi, X. Bao, W. Zhang, D. D. Vos and F.-S. Xiao, *Microporous Mesoporous Mater.*, 2013, **180**, 123-129.

37 R. Kumar, A. Bhaumik, R. K. Ahedi and S. Ganapathy, *Nature*, 1996, **381**, 298-300.

38 Y. Wang, Y. Gao, S. Xie, S. Liu, F. Chen, W. Xin, X. Zhu, X. Li, N. Jiang and L. Xu, *Catal. Today*, 2018, **316**, 71-77.

View Article Online
DOI: 10.1039/C9TA01693G

39 W. Chu, X. Li, S. Liu, X. Zhu, S. Xie, F. Chen, Y. Wang, W. Xin and L. Xu, *J. Mater. Chem. A*, 2018, **6**, 12244-12249.

View Article Online
DOI: 10.1039/C9TA01693G

# Graphical Abstract

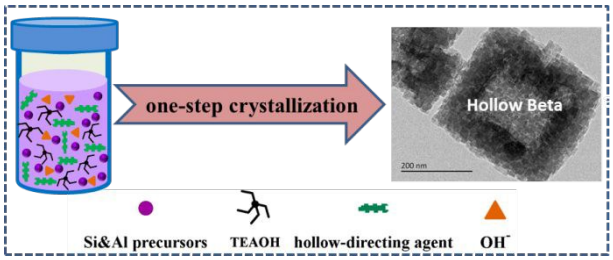


Hollow zeolite Beta can be directly synthesized by using some pentacyclic lactams as hollow-directing agents.